Nonlinear Impedance Spectroscopy of Organic MIS Capacitors and Planar Heterojunction Diodes

Andrew Larsen^a, Ekraj Dahal^b, Justin Paluba^b, Karen Cianciulli^c, Benjamin Isenhart^a, Michael Arnold^a, Bin Du^a, Yu Jiang^a, Matthew S. White^{a,b,*}

^aDepartment of Physics, University of Vermont, 82 University Pl., Burlington, VT 05405
 ^bMaterials Science Program, University of Vermont, 82 University Pl., Burlington, VT 05405
 ^cAsheville School, 360 Asheville School Rd., Asheville, NC 28806

Abstract

We present a nonlinear impedance spectroscopy technique and demonstrate its ability to directly measure nonlinear processes including electron-hole recombination and space charge effects in organic-semiconductor-based diodes and MIS capacitors. The method is based on Fourier analysis of the measured higher harmonic current response to an AC voltage signal. Characterization of the higher harmonic response allows nonlinear impedance spectroscopy to measure material and device properties over a wide range of frequencies, which would otherwise be impossible using conventional impedance spectroscopy. As the higher harmonic signals are purely a product of nonlinear processes, they are independent of the linear device capacitance and resistance. This allows space charge and recombination effects to be investigated at several orders of magnitude higher frequency without fitting to an equivalent circuit model.

1. Introduction

Impedance spectroscopy is a widely used characterization technique for electrochemical and solid-state devices including batteries, fuel-cells, LEDs, and solar cells.[1, 2, 3, 4, 5] The method sources a harmonic wave AC voltage and measures the amplitude and phase of the resulting harmonic current wave. Using Euler's formula to define the voltage and current waves in complex exponential form, the impedance (*Z*) is defined as the ratio of the voltage to the current.

$$V(\omega, t) = V_0 \cos(\omega t) + V_{DC} \tag{1}$$

$$I(\omega, t) = I_0 \cos(\omega t - \phi) + I_{DC}$$
 (2)

$$Z = \frac{V(\omega, t)}{I(\omega, t)} = \frac{V_0}{I_0} (\cos(\phi) + i \sin(\phi))$$
 (3)

Where V_0 and I_0 are the respective amplitudes, ω is the frequency, ϕ is the relative phase difference, and $V_{\rm DC}$ and $I_{\rm DC}$ are the DC offset voltage and current.

Measuring the impedance spectrum by varying the frequency (ω) of the sourced voltage wave over several orders of magnitude allows the behavior of an unknown device to be compared to an equivalent circuit model.[4] Typically, these equivalent circuit models will consist of common circuit elements including resistors, capacitors, and inductors. Models may also include more exotic circuit elements such as constant phase elements and Warburg impedances, which are often associated with diffusion limited, double-layer, or corrosion processes.[6]

Some circuit elements may change as a function of $V_{\rm DC}$. For example, the low frequency resistance of a diode is expected to be proportional to the negative exponential of $V_{\rm DC}$, according to the Shockley diode equation. This creates an inherent problem for impedance spectroscopy of devices: a sourced harmonic voltage wave $V(\omega,t)$ will not result in a pure harmonic current wave $I(\omega,t)$, and the definition of impedance becomes only a first-order approximation in nonlinear systems. The common method to solve this problem is to use a small-signal V_0 , which minimizes the impact of the higher-order signal resulting from the nonlinearities. However, many of the interesting processes in semiconductor devices are nonlinear in nature, including trapping, space-charge-limited current (SCLC), and recombination.[7, 8, 9] Therefore, a direct measurement of the nonlinear processes may be preferable for such devices.

Such analysis will require measurement and characterization of the full Fourier spectrum of the resulting current waveform. We refer the reader to a thorough introduction to the topic by W. Lai[10], but will present a summary of the important points here. A nonlinear response to an applied pure harmonic voltage wave will produce a periodic current signal of the form:

$$I(\omega, t) = \frac{a_0}{2} + \sum_{n=1}^{\infty} a_n \cos(n\omega t) + b_n \sin(n\omega t)$$

$$a_n = \frac{\omega}{\pi} \int_{0}^{2\pi/\omega} I(\omega, t) \cos(n\omega t) dt$$

$$b_n = \frac{\omega}{\pi} \int_{0}^{2\pi/\omega} I(\omega, t) \sin(n\omega t) dt$$
(4)

Preprint submitted to Elsevier June 26, 2018

^{*}Corresponding author

Email address: mwhite25@uvm.edu (Matthew S. White)

Alternatively, this Fourier expansion can be expressed as:

$$I(\omega, t) = \frac{a_0}{2} + \sum_{n=1}^{\infty} A_n \cos(n\omega t + \phi_n)$$

$$a_n = A_n \cos(\phi_n)$$

$$b_n = -A_n \sin(\phi_n)$$
(5)

(Note: The impedance analyzer used in this work measures $|A_n|$ for all frequencies and ϕ_n for frequencies lower than 1500 Hz if n > 1.)

The measured current waveform could be expressed in the Taylor series expansion about the point (V_{DC}, I_{DC}) :

$$I(\omega, t) = I_{DC} + \sum_{n=1}^{\infty} \frac{1}{n!} \frac{d^{n}I}{dV^{n}} \Big|_{V_{DC}} (V(\omega, t) - V_{DC})^{n}$$
 (6)

By combining the expressions in Eq. 5 and Eq. 6, the Fourier coefficients A_n can be expressed in terms of the derivatives of the functional relation between current and voltage. These Fourier coefficients take slightly different forms for the even and odd terms:

$$A_{2n} = \sum_{m=-n}^{\infty} \frac{1}{2^{2m-1}(m-n)!(m+n)!} \frac{\mathrm{d}^{2m}I}{\mathrm{d}V^{2m}} \Big|_{V_{\mathrm{DC}}} V_0^{2m}$$
 (7)

$$A_{2n+1} = \sum_{m=n}^{\infty} \frac{1}{2^{2m}(m-n)!(m+n+1)!} \frac{\mathrm{d}^{2m+1}I}{\mathrm{d}V^{2m+1}} \bigg|_{V_{\mathrm{DC}}} V_0^{2m+1}(8)$$

Analogous to the definition of impedance Z and admittance Y, Y = 1/Z, we define higher-order admittances Y_n such that:

$$\lim_{\omega \to 0} Y_n(\omega) = \frac{\mathrm{d}^n I}{\mathrm{d} V^n} \tag{9}$$

By substituting Y_n in place of $\frac{d^n I}{dV^n}$ in Eq. 7 & 8, we can calculate $Y_n(\omega)$ from the measured $A_n(\omega)$.

If the functional relation is purely linear, then all higher-order derivatives beyond $\frac{dI}{dV}$ go to zero and traditional impedance spectroscopy analysis is perfectly valid. In many semiconductor devices with a nonlinear functional relation, the derivatives of higher order (m) contain relevant information as to the nature of the involved physical processes which produce nonnegligible signal A_m , and in the lower order values of A_n so long as n and m are both either even or odd and n < m. Thin-film organic electronic devices are known to show diode behavior with an exponential dependence of the current on the voltage, transitioning to SCLC with a quadratic dependence at higher forward bias.[11] These two phenomena should be distinguishable as the exponential recombination limited current should produce predictably-spaced A_n , and the transition to SCLC should cause $A_n \to 0$ for all n > 2. For $m \ge 3$, $\frac{\mathrm{d}^m I}{\mathrm{d}V^m}$ should be zero under the quadratic SCLC behavior.

In this work, we demonstrate that these phenomena may be directly characterized over a wide frequency range by sourcing larger amplitude V_0 and measuring the resulting current at all relevant harmonic frequencies. Nonlinear impedance spectroscopy (NLIS) is used to investigate charge transport and recombination in both organic planar heterojunction (PH) diodes

and metal-insulator-semiconductor (MIS) capacitors. The schematics for these two devices are shown in Fig. 1a). The PH diode consists of Al (100 nm), C_{60} (15 nm), copper phthalocyanine (CuPC) (100 nm), molybdenum trioxode (MoO₃) (7nm), and Ag (100 nm). The MIS capacitor is identical in structure, except that the 15 nm C_{60} layer is replaced by 15 nm of anodized aluminum oxide (AlO_x). All device layers are kept as similar as possible to ensure that the hole injection and transport in the CuPC is similar in the two devices, but electron-hole recombination can only occur in the PH diode.

NLIS has been used previously to explore several nonlinear processes, with slight variations in the measurement and analysis procedures. Demonstrated applications of NLIS include nonlinear dielectric spectroscopy[12], characterization of fuel cells[13], field grading insulators[14], diode operation at low frequency[10], interfacial reactions and degradation processes.[15]

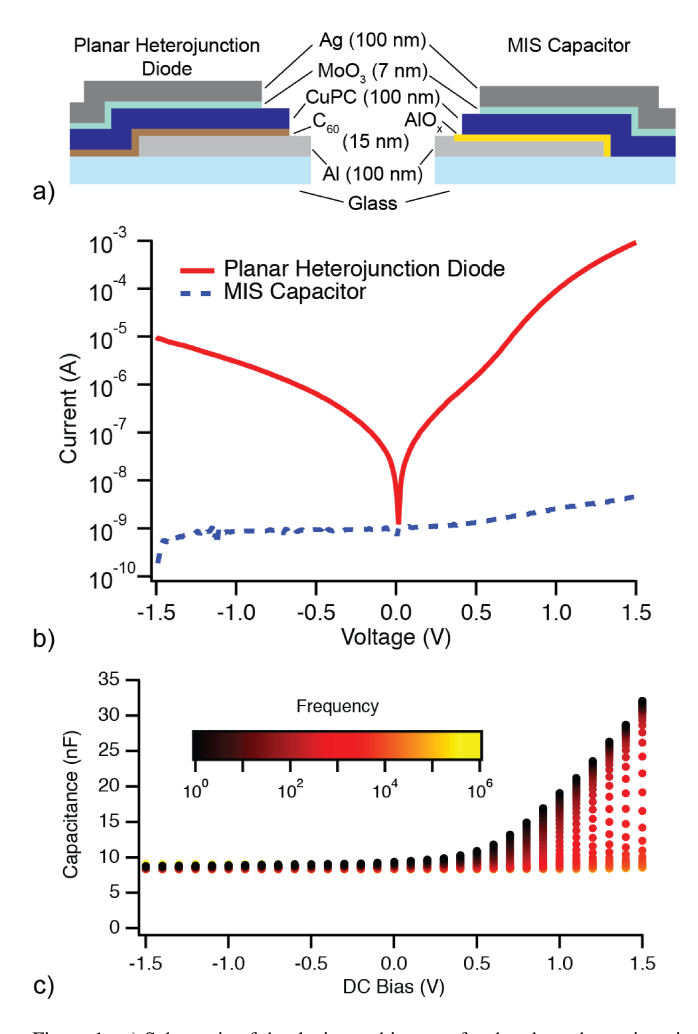


Figure 1: a) Schematic of the device architecture for the planar heterojunction diode and the MIS capacitor. b) DC Current-Voltage curves for the two devices. c) Capacitance-Voltage characteristics of the MIS capacitor from 1 Hz to 500 kHz.

2. Experimental Details

2.1. Materials and Characterization

Copper phthalocyanine and C₆₀ were purchased from Fluka and Aldrich, respectively, and used as received. Glass slides were cut to size and cleaned by sequential ultrasonic bath in water with Equinox detergent, deionized water, acetone, and isopropanol, followed by a 5 min 50 W oxygen plasma cleaning. 100 nm of Al was evaporated onto the glass. The evaporated Al films were anodized in bath of 13.8 mM citric acid in $18 \text{ M}\Omega$ deionized water, with 99.6 mM sodium citrate buffer. A Keithley 2401 Source Measurement Unit was set to source 0.27 mA/cm², for a 3 mm x 20 mm electrode area. The negative electrode was attached to a stainless-steel plate parallel to the Al coated glass, and the positive electrode was attached to the Al. Care was taken that the Al was nearly parallel to the counter electrode. The aluminum was anodized at 5 V, 10 V, 12.5 V and 15 V to create a power vs. AlO_x thickness curve, and the resulting thickness was calculated by evaporating a silver top electrode, generating a capacitor of area 0.0138 cm², and measuring the resulting capacitance with a Novocontrol Alpha-AT frequency response analyzer. We assumed a dielectric constant for AlO_x of 9.34[16] (reported values vary from 7.45 to 14.6 [17, 18]), and used the parallel-plate capacitance to extract a thickness vs. voltage relationship of 1.5 nm/V plus 1.8 nm native oxide.

2.2. Device Fabrication and Measurements

PH diode structures were created by evaporating Al (100 nm), C₆₀ (15 nm), copper phthalocyanine (100 nm), MoO₃ (7 nm), and Ag (100 nm) onto a cleaned glass substrate. Metal-Insulator-Semiconductor (MIS) structures were created by evaporating Al (100 nm) anodized by the procedure described above to form 15 nm of AlO_x , then evaporating copper phthalocyanine (100 nm), MoO₃ (7 nm), and Ag (100 nm). The PH structure was not exposed to air during fabrication. All completed devices were encapsulated between glass slides using UV curable epoxy purchased from Ossila. DC current-voltage response was measured with a Keithley 2401 SMU. Nonlinear impedance analysis was conducted using a Novocontrol Alpha-AT frequency response analyzer. The DC bias was applied to the Ag top electrode, with respect to the Al kept at 0 V. C-V measurements on the MIS capacitors were performed assuming a parallel capacitor/resistor circuit. Measured parallel resistance exceeded 10 $T\Omega$, and serial resistance was below 2Ω . The detection limit for the frequency response analyzer was determined by measuring the higher harmonic NLIS spectrum of a circuit composed of a series resistor with a parallel resistor and capacitor, and defining the magnitude of the measured second harmonic signal of the purely linear system to be the detection limit. Values of the resistors and capacitors were chosen to be close to the PH diode under 0.5 V forward bias when fitting to the equivalent circuit.

3. Results and Discussion

3.1. Impedance Spectroscopy

The organic PH diodes and the MIS capacitors were first subjected to conventional DC current-voltage and linear imp-

edance spectroscopy analysis. The I-V curves of the devices are shown in Fig. 1b). The PH diode shows two orders of magnitude rectification between ± 1.5 V. There is a small, but nonnegligible leakage current indicating either a shunt resistance or low-level electron injection and transport in reverse bias. A distinct diode turn-on region is seen around 0.5 V forward bias, where the current is exponentially proportional to the voltage and is presumably recombination limited. At further forward bias, we see a roll-off commonly associated with the onset of SCLC. These behaviors are highly typical for an organic PH diode.[11, 19, 20]

The I-V curve of the MIS capacitor shows only a small capacitive current due to the voltage sweep, indicating a quality insulating layer blocking DC current in the device. The standard characterization technique for an MIS capacitor is the capacitance-voltage (C-V) measurement. As seen in Fig. 1c), our MIS capacitor shows typical C-V behavior with the capacitance increasing several fold under forward bias, where injected holes can transport through the CuPC and populate the AlO_x interface.[21] This interface is only 15 nm from the underlying Al cathode compared to 115 nm distance between the Al and Ag metal parallel plates. The transition to higher capacitance occurs between 10^3 and 10^4 Hz, depending on the applied DC bias.

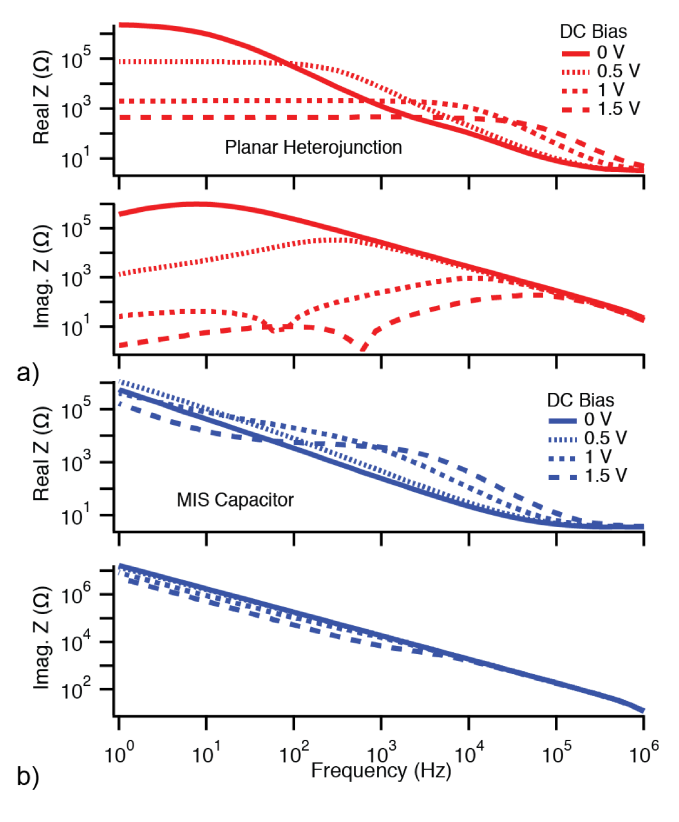


Figure 2: Magnitude of real and imaginary impedance spectra for the a) PH diode and b) MIS capacitor under varying forward DC bias. Impedance spectra were measured using $100~\text{mV}_{rms}$ AC amplitude and conventional linear analysis.

Conventional impedance spectroscopy measures the real and imaginary components of Z as defined in Eq. 3, with ϕ_1 and $|Z| = |V_0/A_1|$. As mentioned above, any nonlinearities produce

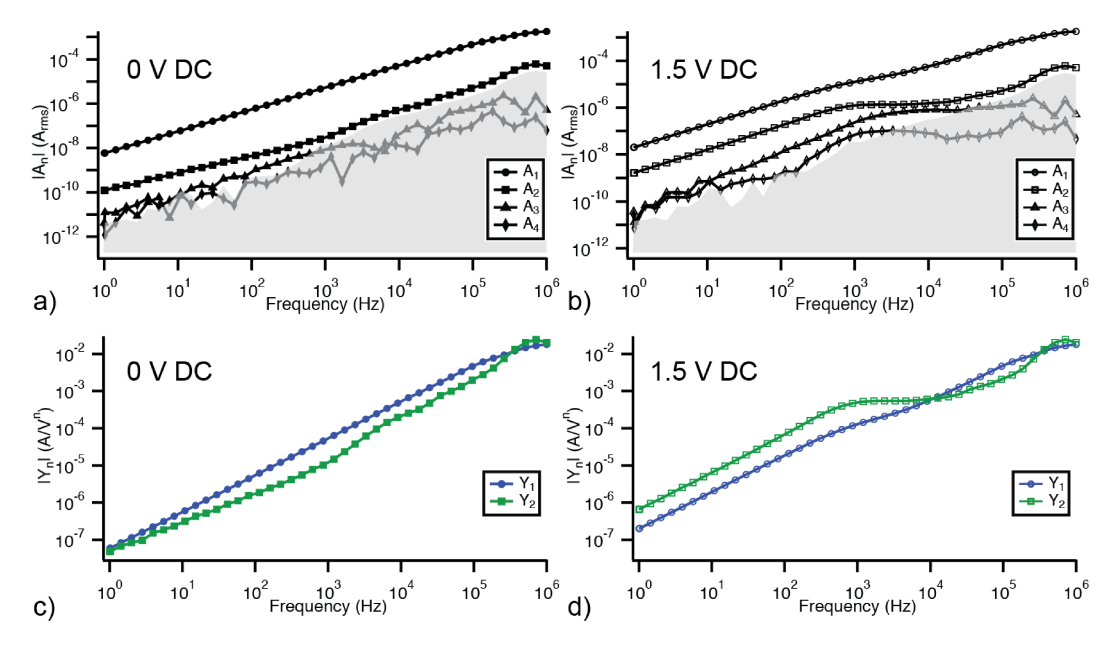


Figure 3: NLIS of the MIS Capacitor under 0 V and 1.5 V bias and 100 mV_{rms} AC amplitude. a) and b) show the measured Fourier Coefficients $|A_n|$. The gray area represents the estimated detection limit of the frequency response analyzer. c) and d) show the calculated $|Y_1|$ and $|Y_2|$.

small deviations with increasing V_0 , but the spectra are largely independent of the amplitude. Fig. 2a) shows the impedance spectrum for the PH diode. The real component shows an expected decreasing impedance at low frequency with increasing forward bias, the signature characteristic of a diode. At high frequencies, the parallel-plate geometry of the thin-film diode results in a capacitive impedance signature. The plot of the imaginary component shows |Im(Z)|, while the sign of Im(Z)is negative due to the capacitive behavior of the device. However, at forward bias greater than 1 V, the imaginary component shows an asymptote in the log-log plot, where Im(Z) goes to zero and becomes positive at low frequencies. Positive imaginary impedance is indicative of inductive behavior, which typically dominates at high frequencies. Therefore, these low frequency inductive signals ("inductive loop" in the Nyquist plot) are a source of much debate in the literature.[22, 23, 24, 25] Working with a simple equivalent circuit model of a capacitor in parallel with a resistor, with or without a series resistor, allows the device capacitance to be calculated as $C = \text{Im}(Y_1/\omega)$. A purely linear analysis in this manner can lead to the conclusion that the low frequency capacitance is negative. [25, 26, 27, 28, 29, 30, 31] Many observations of such behavior have been attributed to nonlinear phenomena. The impact of nonlinear processes in conventional impedance spectroscopy arises from the n = 0, m = 1 term of Eq. 8. By including the first nonlinear correction, the measured A_1 becomes:

$$A_1 = Y_1 V_0 + \frac{1}{8} Y_3 V_0^3 + O(V_0^5)$$
 (10)

These nonlinear corrections should be small if V_0 is also small. However, because Y_3 may be several orders of magnitude larger than Y_1 , the corrections should not be considered as negligible.

The impedance spectrum for the MIS capacitor is shown in Fig. 2b), and we see no evidence of nonlinearities. The impedance appears as would be expected for an MIS capacitor. For a capacitor, $Z=1/i\omega C$, so we see that the log-log plot shows a negative linear dependence with $\log(|\operatorname{Im}(Z)|) = -\log(\omega) + \log(1/C)$. Under forward bias, the transition to a higher C upon carrier injection into the CuPC preserves the slope of -1, but the vertical offset changes.

This conventional impedance spectroscopy analysis reveals consistent behavior for both types of devices explored here. However, it reveals only indirect evidence or no evidence whatsoever of nonlinear processes. Therefore we will focus our discussion on the NLIS analysis described above.

3.2. NLIS of MIS Capacitors

In the MIS capacitor, there are functionally two different operation states. Under reverse or 0 bias, there is little to no injection of holes into the CuPC, and therefore the device behaves primarily as a parallel plate capacitor. Under forward bias, holes are injected into and transported through the CuPC to the AlO_x interface. With the insulating AlO_x preventing electron-hole recombination, any nonlinear processes that may occur in the MIS capacitor will be related to injection into and transport through the CuPC. As conventional impedance analysis provides no measurable indication of nonlinear processes in the MIS capacitor, we turn to NLIS and measure the first four Fourier coefficients. We measured at DC bias spanning ± 1.5 V in 100 mV steps, using AC amplitude V_0 ranging from 6.25 to 200 mV_{rms} by multiples of 2. The effect of AC amplitude variation will be discussed below. We restrict the discussion here to the 100 mV_{rms} amplitude, as this produces strong signal without sampling an overly-large voltage range.

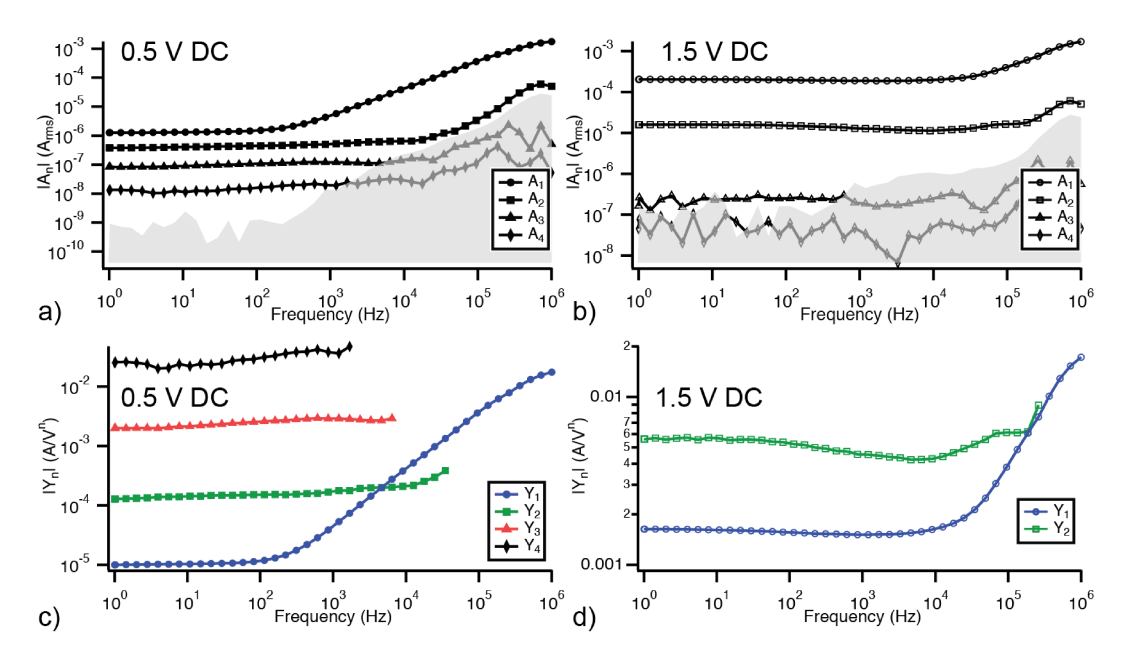


Figure 4: NLIS of the PH Diode under 0.5 V and 1.5 V bias and 100 mV_{rms} AC amplitude. a) and b) show the measured Fourier Coefficients $|A_n|$. The gray area represents the estimated detection limit of the frequency response analyzer. c) and d) show the calculated $|Y_n|$ at frequency ranges where the corresponding $|A_n|$ are significantly within the measurable range.

To explore the nonlinearities in the MIS capacitor in the absence and presence of hole injection, we present an NLIS analysis at 0 V and 1.5 V bias. The measured Fourier coefficients from n = 1 to n = 4 are shown in Fig. 3a) and b). When no external bias is applied, we see that the higher-order coefficients are largely at or below the instrument detection limit. The exception being A_2 , which appears non-negligible for low frequency, and possibly right at the edge of the detection limit for frequencies above 1 kHz. While we do not expect a significant injection current at 0 V bias, the AC sampling range of 100 mV_{rms} may result in asymmetric behavior, resulting in the detected A_2 . We use Eq. 7, 8, and 9 to calculate Y_1 and Y_2 from the measured A_1 and A_2 , which are plotted in Fig. 3c). While Y_1 shows the capacitive behavior, we do not see significant meaningful information in Y_2 . At high frequency (> 10^3 Hz) and at 0 V bias, the calculated Y_2 appears to represent the detection limit for this system. At lower frequency ($< 10^3 \text{ Hz}$), Y_2 is potentially indicative of a small injection current, in agreement with the small variation of low-frequency capacitance around 0 V in Fig. 1c).

Under high forward bias, the higher-order signal becomes significantly more pronounced. In Fig. 3b), it is clear that the measured A_2 is several orders of magnitude above the detection limit for frequencies below roughly 5×10^4 Hz at 1.5 V bias. A_3 and A_4 are also measured above the detection limit in the range from 10^2 to 10^4 Hz, likely due to the change in A_2 . Because of the limited frequency range, and comparatively weak signal, we do not calculate Y_3 and Y_4 . However, when we compare Y_1 and Y_2 in Fig. 3d), we notice a distinct contrast to the 0 V bias signal in Fig. 3c). The hole injection into the CuPC produces the characteristic vertical offset in the linear slope of Y_1 , as discussed above with respect to the impedance spectrum. The NLIS technique reveals that the hole injection and transport

through the CuPC are not ohmic. Below 10^3 Hz, we see a clear Y_2 signal, where Y_3 and Y_4 are below the detection limit. This is indicative of a nonlinear hole transport process with quadratic behavior. Because a similar quadratic signal is observed under high forward bias in the PH diodes discussed below, we suggest that this signal could be due to space-charge limiting distribution of the holes in the bulk of the CuPC. These SCLC processes are of order 2, and would give no contribution to the A_1 measured in conventional impedance spectroscopy, according to Eq. 8.

3.3. NLIS of Planar Heterojunction Diodes

The PH diodes used in this work were designed to be identical to the MIS capacitors, except that electron transport through the C_{60} will enable electron-hole recombination at the C_{60} /CuPC interface. The C_{60} layer is significantly thinner than the CuPC layer, so transport limited current should primarily reflect transport through the CuPC. Transport-limiting processes are expected to dominate at higher forward bias. The measured A_n for the PH diode under 0.5 V and 1.5 V forward bias are shown in Fig. 4a) and b). These two bias points were chosen to represent the recombination-limited and transport-limited current regimes observed in the I-V curve of Fig. 1b).

Under moderate forward bias, where the current is limited by electron-hole recombination, the PH diode should behave according to the Shockley diode equation:

$$I(V) = I_S \left(e^{\frac{V}{nk_B T}} - 1 \right) \tag{11}$$

where I_S is the saturation current and nk_BT is the product of the diode ideality factor and the thermal voltage. We will refer to the diode ideality factor strictly in terms of the product nk_BT to avoid confusion with the index n used throughout this

manuscript. The NLIS spectrum of the PH diode at 0.5 V bias in Fig. 4a) clearly shows significant A_n signal up through the 4th harmonic. This allows for calculation of Y_n for n = 1 to 4, which are shown in Fig. 4c), at frequencies where the corresponding A_n is significantly above the detection limit. At low frequency, these represent the sequential derivatives of the I(V)function, and they display even spacing as would be expected from the factor of $1/nk_BT$ that would separate each exponential function from its derivative. This further allows us to take the ratios Y_n/Y_{n+1} and $\sqrt{Y_n/Y_{n+2}}$ to calculate nk_BT . These calculations are shown in Fig. 5. We see a diode ideality factor of roughly 3, which is higher than one would expect for a p-n or p-i-n diode, but is not uncommon in devices where recombination occurs at a heterojunction interface.[32] The time or frequency bandwidth for measuring recombination dynamics using Y_1 is clearly limited by the RC time constant associated with the parallel-plate nature of the thin film device. However, NLIS allows for comparing the higher-order admittances to characterize electron-hole recombination at one or two orders of magnitude higher frequencies than would be otherwise possible.

At higher forward bias, current in the PH diode is limited by the transport of holes through the bulk of the CuPC. In this SCLC condition, the current obeys the Mott-Gurney square law commonly observed in organic semiconductors[8, 9]:

$$I(V) = \frac{9}{8} \epsilon \mu_h A \frac{(V - V_{bi})^2}{L^3} \tag{12}$$

where ϵ is the dielectric constant of the organic semiconductor, A is the area of the diode, $V_{\rm bi}$ is the built-in potential, and μ_h is the hole mobility. In our planar heterojunction diodes, we do not consider the electron transport through the thin C_{60} layer to be limiting because the layer is over six times thinner and the mobility is known to be three or four orders of magnitude higher than CuPC.[33, 34] NLIS of the PH diode at 1.5 V shown in Fig. 4b) reveals that the Fourier coefficients A_3 and A_4 are near or below the detection limit while a strong, second-order nonlinearity remains. The calculated Y_1 and Y_2 are shown in Fig. 4d). In this situation, only space-charge effects related to

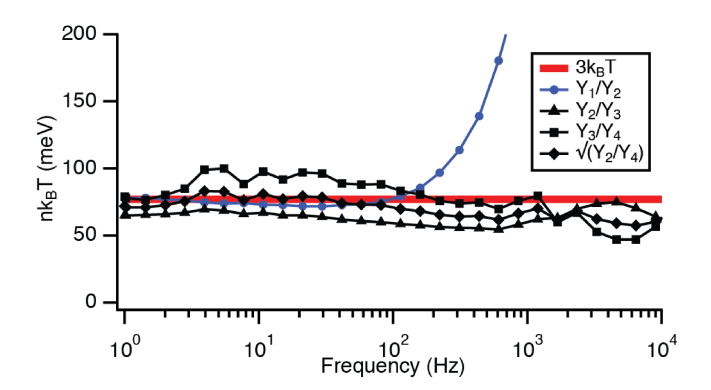


Figure 5: The diode ideality factor, nk_BT , calculated from the ratios of sequential admittances Y_n/Y_{n+1} , and $\sqrt{Y_2/Y_4}$ of the PH diode at 0.5 V bias and 100 mV_{rms} AC amplitude. Y_1 provides limited information at high frequency due to the RC time constant of the parallel plate device. Higher-order Y_n are only sensitive to nonlinear processes like recombination, allowing the ideality factor to be measured at 2 orders of magnitude higher frequency.

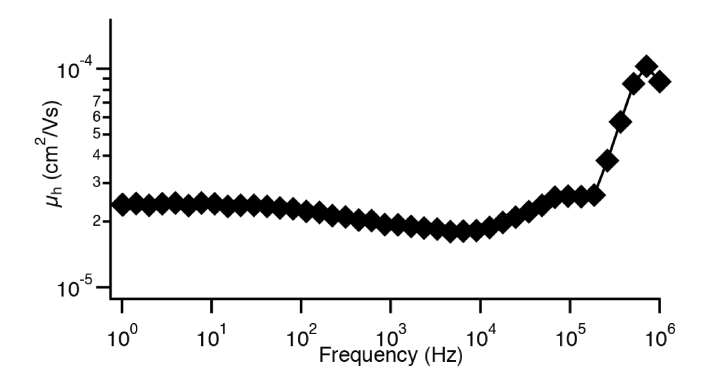


Figure 6: Hole mobility in CuPC estimated by relating the second derivative of the Mott-Gurney law to Y_2 of the PH diode at 1.5 V bias, measured with 100 mV_{rms} AC amplitude.

bulk transport of holes through the CuPC will produce a second order nonlinear signal. The SCLC mobility can be measured at a given DC bias independent of the *RC* time constant by comparing Y_2 to the second derivative of Eq. 12 and solving for μ_h . The relative dielectric constant for CuPC was extracted from the reverse bias dielectric regime[35] of the C-V curve in Fig. 1b using a stacked-dielectric model. The calculated value of $\epsilon = 13.1$ is as expected for CuPC.[36] The hole mobility calculated by NLIS is plotted in Fig. 6, with $\mu_h \approx 2.4 \times 10^{-5}$ cm²/Vs in good agreement with literature values CuPC hole mobility measured by SCLC.[34] Further investigation is required to test if the high-frequency structure is related to current injection transient phenomena.[9]

3.4. Effects of Varying AC Amplitude

As discussed previously, the common method for measuring impedance spectra of nonlinear systems is to reduce the driving amplitude V_0 , sampling only a local voltage regime. It is worthwhile to explore what happens to the NLIS measurement when V_0 is reduced to a small signal. It should be noted that the Fourier coefficients, which are the values measured by any impedance analyzer, do indeed depend on V_0 . This is clearly seen in Eq. 7 & 8. However, the admittance Y_n should be independent of the sampling amplitude. We measured the NLIS spectra of both the MIS capacitor and the PH diode through our full DC bias range using V_0 ranging from 6.25 mV_{rms} to 200 mV_{rms} by multiples of 2.

The calculated Y_n for the PH diode at 0.5 V forward bias are shown in Fig. 7. Our measured Y_n are largely independent of V_0 . However, we do see that the higher-order admittances are influenced heavily by the instrument detection limit. When the A_n signal approaches the detection limit, the corresponding Y_n signal becomes noisy. Once A_n falls below the detection limit, the calculated Y_n begins to drift significantly as V_0 becomes small. This noise and signal drift due to instrument sensitivity are dependent on the measurement frequency. The higher-order Fourier coefficients are inherently harder to detect as the V_0^n factor makes them small. As an example, the noise that appears as A_3 approaches the detection limit is visible in Fig. 7c) with $V_0 = 25$ mV_{rms}. Smaller V_0 causes the calculated Y_3 to drift significantly from the high amplitude values. Note

that the $Y_3V_0^3$ correction term in A_1 may still very well be influencing the signal when A_3 is below the instrument detection limit. This is due to a combination of instrument sensitivity at ω vs. 3ω , and the fact that the pre-factor is 3 times larger, 1/8 compared to 1/24.

4. Conclusions

We present an impedance spectroscopy analysis of nonlinear processes in organic electronic devices using Fourier analysis of the measured response at higher harmonic frequencies. This NLIS technique is shown to be capable of resolving nonlinear phenomena over a wide frequency range, with the upper limit of roughly 10⁵ Hz, and the lower limit determined by the

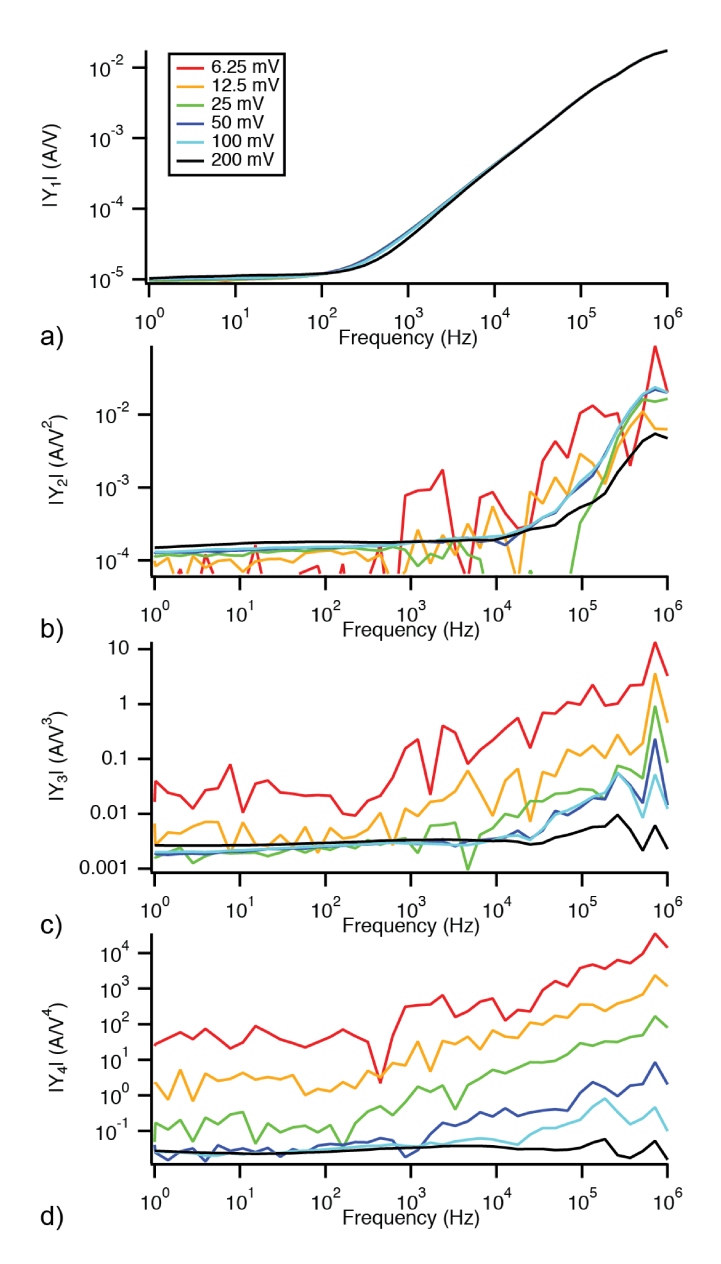


Figure 7: a) $|Y_1|$, b) $|Y_2|$, c) $|Y_3|$, and d) $|Y_4|$ for the PH diode at 0.5 V DC bias, with AC amplitude ranging from 6.25 to 200 mV_{rms}. Variations of $|Y_n|$ as a function of V_0 are indicative of the instrument detection limit.

patience of the operator and the durability of the device under test to withstand prolonged operation. NLIS provides several advantages over conventional impedance analysis for exploring such nonlinear processes. The inherent advantage is that it does not assume linear response for the analysis. Perhaps the biggest experimental benefit of NLIS is that purely resistive and capacitive processes do not contribute to the A_n Fourier coefficients for $n \geq 2$, allowing direct characterization of nonlinear processes at frequencies where RC time constants may otherwise preclude measurement.

Comparing the signal magnitude of the higher harmonic Fourier coefficients allows for clear determination of the nature of the nonlinear process. Recombination limited current in the PH diode produced higher-order admittances that were proportional to each other, and the constant of proportionality was used to determine the diode ideality factor over a wide frequency range. Space charge effects in the bulk of the CuPC were found to produce quadratic dependence of the current on voltage in both PH diodes and MIS capacitors, allowing the determination of the hole mobility. In contrast to the conventional approach for impedance spectroscopy, NLIS allows for direct characterization of nonlinear processes in the frequency domain.

Acknowledgements

This material is based upon work supported by the National Science Foundation under Grant No. OIA-1738575. A. Larsen is grateful for support from the UVM Office of Fellowships, Opportunities, and Undergraduate Research (FOUR) Clean Energy Summer Research Fellowship. Y. Jiang, M. Arnold, and B. Du are grateful to the UVM FOUR and Department of Physics for support from the UVM FOUR Mini Grant program and the Department of Physics Crowell Summer Research Award. J. Paluba and E. Dahal are grateful for support from the UVM Clean Energy Fund Innovation Award. M. White, Y. Jiang, and B. Du are grateful to the University of Vermont Office of the Vice President for Research for support through the OVPR EXPRESS Grant.

References

- [1] J. Bisquert. Theory of the Impedance of Electron Diffusion and Recombination in a Thin Layer. *Journal Of Physical Chemistry B*, 106(2):325–333, 2002.
- [2] J. R. Macdonald. Impedance Spectroscopy and its Use in Analyzing the Steady-State AC Response of Solid and Liquid Electrolytes. *Journal of electroanalytical chemistry and interfacial electrochemistry*, 223(1):25–50, 1987.
- [3] I. H. Campbell, D. L. Smith, and J. P. Ferraris. Electrical-Impedance Measurements of Polymer Light-Emitting-Diodes. *Applied Physics Letters*, 66(22):3030–3032, 1995.
- [4] A. Pitarch, G. Garcia-Belmonte, I. Mora-Sero, and J. Bisquert. Electro-chemical Impedance Spectra for the Complete Equivalent Circuit of Diffusion and Reaction Under Steady-State Recombination Current. *Physical Chemistry Chemical Physics*, 6(11):2983–2988, 2004.
- [5] N. Wagner, W. Schnurnberger, B. Müller, and M. Lang. Electrochemical Impedance Spectra of Solid-Oxide Fuel Cells and Polymer Membrane Fuel Cells. *Electrochemica Acta*, 43(24):3785–3793, August 1998.
- [6] J. Kowal, D. Hente, and D. U. Sauer. Model Parameterization of Non-

- linear Devices Using Impedance Spectroscopy. *IEEE Transactions On Instrumentation And Measurement*, 58(7):2343–2350, July 2009.
- [7] W. L. Leong, S. R. Cowan, and A. J. Heeger. Differential Resistance Analysis of Charge Carrier Losses in Organic Bulk Heterojunction Solar Cells: Observing the Transition from Bimolecular to Trap-Assisted Recombination and Quantifying the Order of Recombination. Advanced Energy Materials, 1(4):517–522, May 2011.
- [8] P. W. M. Blom, M. J. M. De Jong, and M. G. Van Munster. Electric-Field and Temperature Dependence of the Hole Mobility in Poly (p-phenylene vinylene). *Physical Review B*, 55(2):R656, 1997.
- [9] M. A. Lampert and P. Mark. Current Injection in Solids, 1970.
- [10] W. Lai. Fourier Analysis of Complex Impedance (Amplitude and Phase) in Nonlinear Systems: A Case Study of Diodes. *Electrochimica Acta*, 55 (19):5511–5518, July 2010.
- [11] P. W. M. Blom and M. J. M. De Jong. Electrical Characterization of Polymer Light-Emitting Diodes. *IEEE Journal Of Selected Topics In Quantum Electronics*, 4(1):105–112, 1998.
- [12] Y. Ishibashi. Nonlinear Dielectric Spectroscopy. *Journal of the Korean Physical Society*, 32:S407–S410, February 1998.
- [13] J. R. Wilson, D. T. Schwartz, and S. B. Adler. Nonlinear Electrochemical Impedance Spectroscopy for Solid Oxide Fuel Cell Cathode Materials. *Electrochimica Acta*, 51(8-9):1389–1402, January 2006.
- [14] L. Almquist. Nonlinear Impedance Spectroscopy. Master's thesis, Chalmers University of Technology, Gothenburg, Sweden, December 2015.
- [15] T. J. McDonald and S. Adler. Theory and Application of Nonlinear Electrochemical Impedance Spectroscopy. ECS Transactions, 45(1):429–439, April 2012.
- [16] K. F. Young and H. P. R. Frederikse. Compilation of the Static Dielectric Constant of Inorganic Solids. *Journal of Physical and Chemical Reference Data*, 2(2):313–410, April 1973.
- [17] M. M. Lohrengel. Thin Anodic Oxide Layers on Aluminum and Other Valve Metals - High-Field Regime. *Materials Science & Engineering R-Reports*, 11(6):243–294, 1993.
- [18] A. I. Mardare, M. Kaltenbrunner, N. S. Sariciftci, S. Bauer, and A. W. Hassel. Ultra-thin anodic alumina capacitor films for plastic electronics. physica status solidi (a), 209(5):813–818, April 2012.
- [19] C. W. Tang. Two-Layer Organic Photovoltaic Cell. Applied Physics Letters, 48(2):183–185, 1986.
- [20] C. W. Tang and S. A. VanSlyke. Organic Electroluminescent Diodes. Applied Physics Letters, 51(12):913, 1987.
- [21] E. Itoh and K. Miyairi. Interfacial Charge Phenomena at the Semiconductor/Gate Insulator Interface in Organic Field Effect Transistors. *Thin Solid Films*, 499(1-2):95–103, March 2006.
- [22] J. Fleig, J. Jamnik, J. Maier, and J. Ludvig. Inductive Loops in Impedance Spectroscopy Caused by Electrical Shielding. *Journal Of The Electrochemical Society*, 143(11):3636–3641, 1996.
- [23] K. S. A. Butcher, T. L. Tansley, and D. Alexiev. An Instrumental Solution to the Phenomenon of Negative Capacitances in Semiconductors. *Solid-State Electronics*, 39(3):333–336, 1996.
- [24] J. H. Werner. Negative Capacitance at Metal-Semiconductor Interfaces -Comment. *Journal of Applied Physics*, 70(2):1087–1088, 1991.
- [25] X. Wu, E. S. Yang, and H. L. Evans. Negative Capacitance at Metal-Semiconductor Interfaces. *Journal of Applied Physics*, 68(6):2845–2848, 1990
- [26] L. S. C. Pingree, B. J. Scott, M. T. Russell, T. J. Marks, and M. C. Hersam. Negative Capacitance in Organic Light-Emitting Diodes. *Applied Physics Letters*, 86(7):073509, 2005.
- [27] T. Misawa. Impedance of Bulk Semiconductor in Junction Diode. *Journal Of The Physical Society Of Japan*, 12(8):882–890, 1957.
- [28] C. H. Champness and W. R. Clark. Anomalous Inductive Effect in Se-Metal Contacts. Applied Surface Science, 48-9:337–342, 1991.
- [29] E. Ehrenfreund, C. Lungenschmied, G. Dennler, H. Neugebauer, and N. S. Sariciftci. Negative Capacitance in Organic Semiconductor Devices: Bipolar Injection and Charge Recombination Mechanism. *Applied Physics Letters*, 91(1):012112, 2007.
- [30] C. Lungenschmied, E. Ehrenfreund, and N. S. Sariciftci. Negative Capacitance and its Photo-Inhibition in Organic Bulk Heterojunction Devices. *Organic Electronics*, 10(1):115–118, 2009.
- [31] J. Bisquert, G. Garcia-Belmonte, A. Pitarch, and H. J. Bolink. Negative Capacitance Caused by Electron Injection Through Interfacial States in

- Organic Light-Emitting Diodes. *Chemical Physics Letters*, 422(1-3):184–191, 2006.
- [32] C. R. Miskys, J. A. Garrido, C. E. Nebel, M. Hermann, O. Ambacher, M. Eickhoff, and M. Stutzmann. AlN/Diamond Heterojunction Diodes. *Applied Physics Letters*, 82(2):290–292, January 2003.
- [33] Th. B. Singh, N. Marjanović, G. J. Matt, S. Günes, N. S. Sariciftci, A. Montaigne Ramil, A. Andreev, H. Sitter, R. Schwodiauer, and S. Bauer. High-mobility n-channel organic field-effect transistors based on epitaxially grown C₆₀ films. *Organic Electronics*, 6(3):105–110, June 2005
- [34] R. F. Salzman, J. Xue, B. P. Rand, A. Alexander, M. E. Thompson, and S. R. Forrest. The Effects of Copper Phthalocyanine Purity on Organic Solar Cell Performance. *Organic Electronics*, 6(5-6):242–246, December 2005.
- [35] C.-H. Kim, Y. Bonnassieux, and G. Horowitz. Compact DC Modeling of Organic Field-Effect Transistors: Review and Perspectives. *Electron Devices, IEEE Transactions on*, 61(2):278–287, January 2014.
- [36] N. Shi and R. Ramprasad. Intrinsic dielectric properties of phthalocyanine crystals: An *ab initio* investigation. *Physical Review B*, 75(15):2488–7, April 2007.